IET Science, Measurement & Technology

Evaluation of Strand-to-Strand Capacitance and Dissipation Factor in Thermally Aged Enameled Coils for Low Voltage Electrical Machines

Vincenzo Madonna [1], Paolo Giangrande[1*], Michael Galea [1,2]

[1] Power Electronics Machines and Control Group, University of Nottingham, Nottingham NG7 2RD, U.K.
[2] School of Aerospace, University of Nottingham Ningbo China, Ningbo 315100, China
[*] p.giangrande@nottingham.ac.uk

Abstract: The dissipation factor (i.e. tanδ) and insulation capacitance measurements are conventional monitoring methods for assessing the aging level of insulation systems. Knowing these quantities, provides an invaluable indication of the dielectric losses within the insulating materials. However, how these values are effected by the aging processes due to thermal stresses has until today never been investigated fully. Thus, this paper studies the influence of thermal aging on the tanδ and insulation capacitance of windings for electrical machines. The work is done for class 200, round enameled magnet wire specimens. The study aims at improving the design process of electrical machines for short duty cycle applications; hence, its outcome might be included at the design stage for enhancing reliability and lifetime. Random wound coils are chosen in the performed study, because they are the most common winding arrangement for low voltage electrical machines, which are employed in a wide range of applications (e.g. from home appliances to aerospace motors). Based on the collected data, considerations regarding the impact of relative humidity on both dissipation factor and insulation capacitance are presented. Finally, the correlation between the partial discharge inception voltage and the diagnostic measurements is experimentally verified.

1. Introduction

One of the key components or sub-system of an electrical machine (EM) is the winding. Low voltage (i.e. below ~1000 V) EMs generally adopt windings manufactured with round enameled wires (i.e. magnet wire), which are randomly wound [1]. The insulation between two turns belonging to the same coil is provided through a thin layer of insulating enamel, whose chemical composition features an organic nature (i.e. Type I insulation) [2]. Low voltage EMs are found in a wide range of applications, including industrial, home appliances and transportation [3-5]. The latter are particularly demanding in terms of insulation capability to withstand elevated level of stresses, such as thermal, electrical, mechanical and environmental [6-8]. The thermal stress represents one of the main aging factors in electric transportation applications, where a significant level of power density is often required [9]. Indeed, the EM's power to weight ratio is normally constrained by the maximum temperature at which the insulating materials can be operated (i.e. thermal class) [10]. At the same time, EMs for transportation applications are expected to be highly reliable during their whole lifetime. Inter-turn insulation degradation, induced by excessive thermal aging, is recognized as one of the major causes of premature failure in low voltage EMs [11, 12]. Evaluating the deterioration level, and thus being able to predict the useful lifetime of inter-turn insulation, is crucial, particularly for EMs employed in safety-critical applications [13].

For medium and high voltage EMs, equipped with Type II insulating materials (i.e. mixed organic-inorganic materials), several tools are nowadays available for determining the insulation's aging state [1, 14]. These include both on-line and off-line techniques. Among the off-line strategies, the dissipation factor (or tanδ) measurement is frequently implemented for EMs [15-18]. In fact, this test allows to assess the global condition of phase-to-ground insulation [18], as it is an accurate indicator of partial discharges (PDs) activity. Alternative non-destructive tests performed on low voltage EMs include insulation resistance, insulation capacitance (IC) and PD measurements [11, 19, 20]. In general, these methods can evaluate the aging level of phase-to-ground and/or phase-to-phase insulation systems. The on-line and off-line PD tests can be used to detect the occurrence of PDs in the inter-turn insulation [21-23]. Nonetheless, it is well recognized that in Type I insulation, the PDs inception usually corresponds to the insulation's end-of-life [24, 25].

In [19], an on-line, non-intrusive approach is proposed for quantifying the thermal aging of inter-turn insulation in low voltage EMs. The analysis is based on accelerated tests carried out on enameled wire twisted pairs, by using an ventilated oven (i.e. thermal exposure at constant temperature). A similar study, but for medium voltage EMs is discussed in [26], where the thermal aging of the phase-to-ground insulation is correlated with changes of IC, dissipation factor and PD patterns. The impact of the thermal aging on the IC is also examined in [27], where the aged specimens are twisted pairs and the thermal aging is associated with the reduction of partial discharge inception voltage (PDIV).

In this paper, the effect of the thermal aging on an enameled magnet wire is considered. The insulation system under analysis consists of two insulating material layers (i.e. double enamel magnet wire), respectively made of modified polyester (i.e. base coating) and polyamide-imide (i.e. over-coating). The investigation is experimentally performed on random wound coils, since they are the most common winding arrangement in low voltage EMs. The thermal aging of the stand-to-strand (i.e. turn-to-turn) insulation is assessed by measuring both the IC and tanδ values, for extrapolating the relationship between aging stress and diagnostic quantities. The aging process is accelerated through the application of a periodic thermal profile (i.e. thermal exposure at variable

temperature), which is obtained exploiting the Joule effect. Its temperature range is above the insulation thermal class (i.e. 200°C), with the purpose of shortening the testing campaign. In terms of thermal stress, a variable temperature profile is preferred to a constant temperature, because the former is representative of the actual condition experienced by high-performance EMs, when they are thermally overloaded for short time periods (e.g. EMs for aerospace and automotive applications [28, 29]). Particular attention is focused on humidity throughout the experimental campaign. Indeed, humidity is recorded during IC and tanδ measurements and its influence is discussed in the paper. In order to experimentally prove the correlation between PD activity and diagnostic measurements (i.e. tanδ and IC), the PDIV is finally measured via a commercial PD detector. The collected data are a valuable source of information for the EMs designers. In fact, the findings of the presented work can be used for designing low voltage EMs, which are intended to be operated above the thermal class, in order to increase their power density without compromising the machine availability.

2. Theoretical Background

An ideal insulating material behaves as a lossless capacitor; hence, if a sinusoidal voltage is applied across the insulation, the resulting current leads the voltage by an angle of 90 degrees (i.e. purely capacitive current). On the other hand, real insulating materials exhibit dielectric losses. Thus, when they are subject to a sinusoidal voltage, the produced current leads the voltage by an angle that is equal to 90 degrees minus δ, where δ is defined as the dielectric loss angle [18, 30].

Assuming a sinusoidal excitation, the non-ideal dielectric is characterized by a complex relative permittivity ε_r^*, described as in (1), where ε_r' is the relative permittivity (i.e. real part), which is related to the energy stored inside the insulating material, while ε_r'' (i.e. imaginary part) is the relative loss index, also known as loss factor, since it is associated to the energy dissipated within the insulating material [30].

$$\varepsilon_r^* = \varepsilon_r' - j\varepsilon_r'' \tag{1}$$

The stored energy ε_r'' is an indicator of the material attitude to be polarized due to the electric field. Both ε_r' and ε_r'' are frequency-dependent through a number of intricate dielectric relaxation and polarization phenomena [31]. Considering on-field operations, very low frequency measurements (i.e. 0.01 – 0.1 Hz range) are often conducted for practical convenience, because low frequency requires reduced power, leading to compact testing devices. All the results reported hereafter refer to measurements performed in a laboratory environment, at 50 Hz frequency and controlled ambient temperature (more details regarding the test procedure are provided in Section 3.3).

As shown in Fig. 1 (a), a non-ideal insulation is schematically modelled by an ideal capacitor C in parallel to a resistor R, accounting for the dielectric losses. In case the non-ideal insulation is excited with a sinusoidal voltage, the ensuing vector diagram of the parallel circuit is similar to the one in Fig. 1 (b). The dielectric dissipation factor is defined as the tangent of the dielectric loss angle δ (i.e. tanδ). Hence, it can be calculated as the ratio between the resistive current I_R and the capacitive current I_C, or as the ratio between the imaginary and real parts of the complex relative permittivity. Both these expressions are given by (2).

$$tan\delta = \frac{I_R}{I_C} = \frac{\varepsilon_r''}{\varepsilon_r'} \tag{2}$$

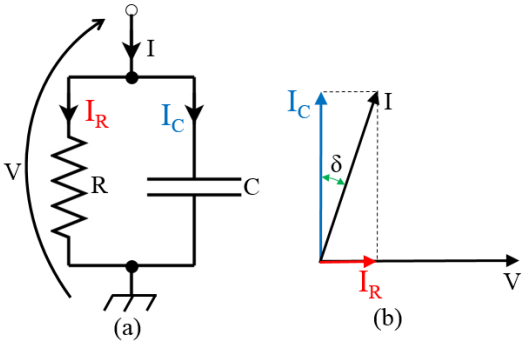

Fig. 1. *Non-ideal insulating material model*: ***(a)*** *circuit schematic and* ***(b)*** *vector diagram.*

Further, the dielectric loss is the sum of solid losses (i.e. conduction and polarization losses) and ionization losses (i.e. losses due to the inception of PDs) [15, 18] therefore, for small values of δ, the tanδ is determined by (3), where $tan\delta_S$ is the term accounting for solid losses, whilst $tan\delta_{PD}$ is the ionization losses term.

$$tan\delta = tan\delta_S + tan\delta_{PD} \tag{3}$$

By applying a potential difference (i.e. excitation voltage) across two electrodes, separated by a solid insulating material, an electric field occurs within the dielectric. If the dielectric is characterized by air inclusions (i.e. voids), and the electric field's magnitude is below the dielectric strength of air (i.e. *≈3kV/mm* at sea level pressure), the ionization process will not arise. As long as the insulation's voids are not ionized, the tanδ value will be only dependent on the solid losses term (i.e. $tan\delta = tan\delta_S$) [16]. In this condition, the measured tanδ is only slightly influenced by the excitation voltage used during the measurement [15, 16, 18]. When the excitation voltage is increased and the developed electric field is such that voids begin to become ionized (i.e. PDs are incepted), the term $tan\delta_{PD}$ will steeply rise along with the excitation voltage, as illustrated in Fig. 2 [18]. The voltage value inducing PDs inception is commonly called ionization voltage, corona inception voltage or PDIV [18]. The difference between the tanδ at two designated voltages (i.e. tanδ tip-up, Δtanδ or differential tanδ) quantifies the amount of dielectric loss within the insulation, thus it is an indirect measurement of PD activity [1, 15, 18].

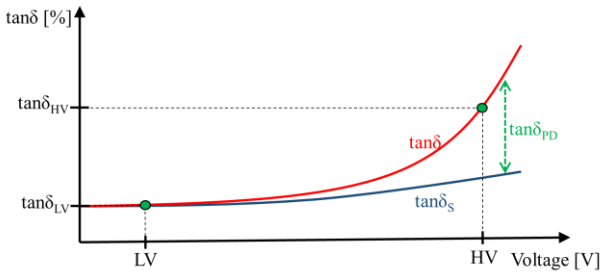

Fig. 2. *Test voltage influence on the tanδ measurement.*

Using the nomenclature reported in Fig. 2, the differential tanδ can be calculated according to (4).

$$\Delta tan\delta_{(HV-LV)} = tan\delta_{HV} - tan\delta_{LV} \tag{4}$$

The same behavior, as for the tanδ detection, can be noticed on the IC measurement, since its value boosts at higher excitation voltages. The IC raise indicates that the insulation voids are ionized, therefore the effective thickness of the insulation is reduced causing an increment on the measured strand-to-strand IC [1].

3. Test Setup and Procedure

3.1. Specimens Description

The analyzed specimens are coils wound with a class 200 round enameled magnet wire. A double enamel layer, namely a modified polyester base coat and a polyamide-imide over coat, forms the wire insulation. The chosen specimen's arrangement (i.e. random wound coil) is the configuration usually adopted for the windings of low voltage EMs [32]. Hence, it is more representative of the actual application, compared with other traditional specimen's topologies (e.g. twisted pairs). Every coil features 20 turns in total and it is composed by two sub-coils in parallel (i.e. strands). This layout allows to easily measure the strand-to-strand dielectric properties (i.e. tanδ and IC). The coil's turns are kept together using Kapton® tape for mechanical purpose only. An unaged coil is shown in Fig. 3, whereas further details about the specimens are listed in Table 1.

Fig. 3. *Unaged coil employed for the investigation.*

Table 1 Specimens Characteristics

Parameter	Quantity
Thermal class	200
Number of turns	20
Strands in parallel	2
Copper core diameter	0.4 mm
Average turn length	250 mm

3.2. Test Setup

The block diagram of the test setup is sketched in Fig. 4. The technical standards for insulation thermal qualification suggest to utilize a minimum of 10 specimens for twisted pairs and at least 5 specimens for motorettes [33, 34]. As no recommendations exist for random wound coils, then 12 series connected coils were considered to be an appropriate number (i.e. statistically representative population of samples) for the accelerated aging tests. The coils are fed by a DC current, and thus heated up exploiting the Joule effect. The DC power supply is controlled via an external DSP through the analogue interface. The coils' temperature is measured by means of K-type thermocouples, whose output signal is amplified and elaborated using the DSP. The specimens are hung on a PTFE rod and inserted inside a fume hood featuring a variable air flow-rate, as depicted in Fig. 5. The temperature profile applied to the series connected coils is obtained and controlled by selecting the suitable combinations of DC current and air flow-rate values.

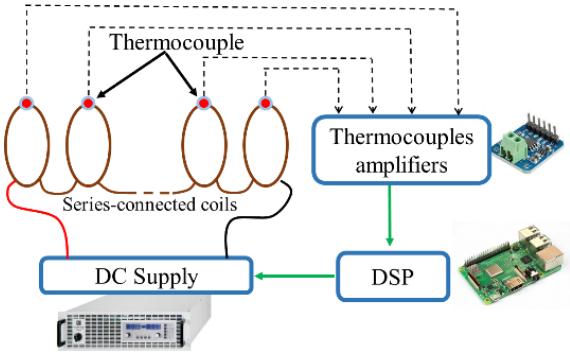

Fig. 4. *Block diagram of the experimental setup.*

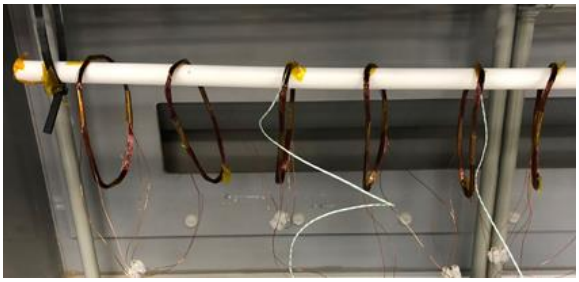

Fig. 5. *Specimens' arrangement: coils hung inside a fume hood.*

To accelerate the thermal degradation of the specimens, a temperature higher than the insulation thermal class is selected for the aging cycles. The implemented temperature profile ranges from a minimum of 200°C to a maximum of 280°C, whilst its time period is equal to 77 s, as detailed in Fig. 6. A thermal stress at variable temperature has been purposely preferred to a constant temperature aging, because the major aim of the presented study consists in investigating the insulation behavior of EMs, while thermally overloaded for a short time period. Having a temperature varying in a wide range might trigger multiple sources of degradation. Also, severe mutations at molecular level might be induced, especially in Type I insulating materials (e.g. breakage of polymer bonds). Although the chosen thermal stress deviates from the standards recommendations [33], this is justified by the fact that it mirrors the actual operating conditions of EMs under heavy overloads.

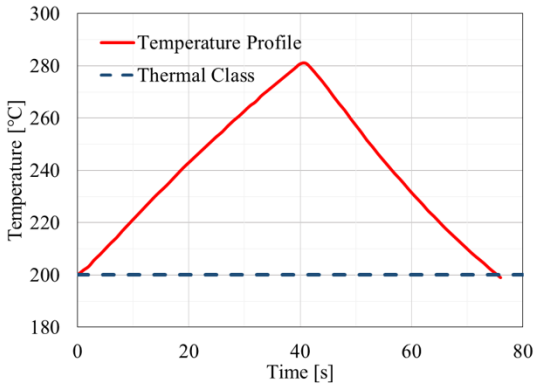

Fig. 6. *Temperature profile for the accelerated aging cycles.*

3.3. Test Procedure

Having defined the temperature profile, the coils are thermally aged making use of the above-mentioned experimental setup. Every 24 hours (i.e. 2186 cycles), the thermal exposure is stopped, and the strand-to-strand insulation conditions are checked through diagnostic measurements. The strand-to-strand IC and tanδ values are recorded for each specimen via a Megger® Delta 4000. Both measurements (i.e. IC and tanδ) are carried out at a fixed frequency of 50 Hz and they are repeated for different excitation voltages ranging from 20 to 500 V rms, with a 20 V step. After a preliminary test campaign, it was observed that the unaged specimens revealed tanδ values constant up to an excitation voltage of 480-500 V rms. Therefore, the excitation voltage of 500 V rms is assumed as upper limit value for the diagnostic. The thermal test continues until the insulation breakdown is detected (i.e. tripping of Megger® generator). When a specimen fails, it is removed from the experiment and the time to failure is recorded. Fig. 7 reports the flow-chart of the test procedure for a generic specimen. The diagnostic measurements are performed at controlled ambient temperature (i.e. 23°C ± 1°C) and uncontrolled relative humidity (RH). Hence, the RH values are acquired at each diagnostic session by means of a hygrometer and the collected results are summarized in Fig. 8 and Fig. 9. Referring to these figures, the cycle identified as '0' represents the preliminary diagnostic measurement (i.e. before the thermal aging), which is conducted without any specimens' pre-conditioning.

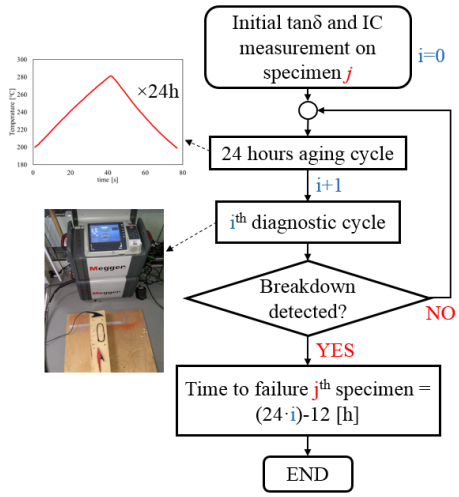

Fig. 7. *Flow-chart of the testing procedure.*

To evaluate the RH influence on the diagnostic measurements (i.e. IC and tanδ), two additional coils are wound and kept unaged throughout the whole test campaign. These two 'reference specimens' are characterized by the same layout as the coils thermally aged (i.e. 2 strands with 20 turns each) and their strand-to-strand IC and tanδ values are assessed at the beginning of every diagnostic session. Any change detected on the aforementioned measurements is to be solely ascribed to the RH variation, since the 'reference specimens' are not thermally stressed. Due to the short duration of the whole diagnostic session (i.e. <60 minutes), it is reasonable to assume constant the RH during the measurements. In Fig. 8, the strand-to-strand IC of one 'reference specimen' is plotted against the corresponding diagnostic cycle (i.e. black continuous line) and its percent variation, results lower than 5% throughout the whole diagnostic session. Thus, it can be said that the IC measurements are only slightly influenced by the ambient RH variability. On the contrary, the tanδ values are strongly affected by the RH and significant changes are witnessed on the 'reference specimens'. This can be observed in Fig. 9, where the %tanδ of just one 'reference specimen' is mapped at each diagnostic cycle. The %tanδ varies between 0.18 and 0.75 and this is due only to the effect of the ambient RH. Considering this, then a proportional relationship between %tanδ and RH% can be perceived from the findings shown in Fig. 9.

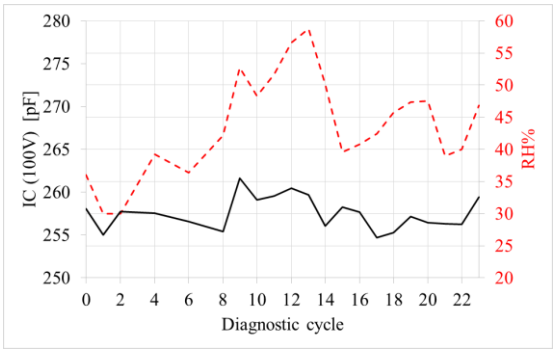

Fig. 8. *RH influence on the diagnostic measurements: 1) IC of 'reference specimen' at 100 V rms (black continuous line) and 2) measured RH% (red dashed line).*

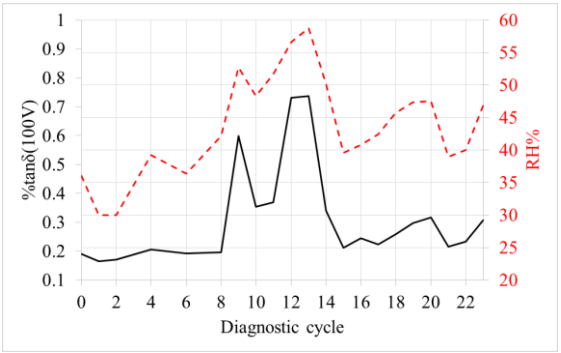

Fig. 9. *RH influence on the diagnostic measurements: 1) %tanδ of 'reference specimen' at 100 V rms(black continuous line) and 2) measured RH% (red dashed line).*

4. Results and Discussion

4.1. Insulation Capacitance

As previously mentioned, before starting the thermal accelerated aging cycles, the strand-to-strand IC of all the unaged specimens is measured at 50 Hz for several excitation voltages within the range 20÷500 V rms (using 20 V rms step). Since the coils are randomly wound, the gathered IC values reveal a significant variability for a given excitation voltage. For example, the strand-to-strand IC values vary in the range of 250-350 pF, when 100 V rms excitation voltage is applied.

Due to the thermal aging, an increment on the strand-to-strand IC is seen in the 12 specimens tested. This behavior is visualized in Fig. 10, where the IC values measured at a fixed voltage amplitude of 100 V rms are plotted against the number of aging cycles. For representation clarity, only 4 specimens (i.e. S1÷S4) are shown in Fig. 10, while the voltage amplitude of 100 V rms is chosen, because

it is well below the PDIV. The purpose of Fig. 10 is to highlight the thermal aging influence on the strand-to-strand IC, without accounting for PD activity.

In order to identify the statistical distribution, which best fits the recorded IC data, a post-processing exercise can be carried out. The outcome of this analysis is summarized in Fig. 11, where four different probability distributions are presented (i.e. Weibull, exponential, normal and lognormal). Among these, the lognormal distribution is the most appropriate for fitting the collected strand-to-strand IC values.

A complete overview of the strand-to-strand IC trend with the thermal degradation is depicted in Fig. 12. In fact, assuming a lognormal distribution, the average value of the strand-to-strand IC increment (in percent) is calculated for the 12 specimens, together with the standard deviation. From Fig. 12, it can be observed that the strand-to-strand IC value rises rapidly during the first two aging cycles. After those early thermal exposures, the IC value keeps increasing, but with a lower slope. As expected, the standard deviation becomes greater with the number of diagnostic sessions, due to the number of specimens decrement throughout the test campaign. The specimens' failure times are listed in Table 2, where they are organized in an ascending order.

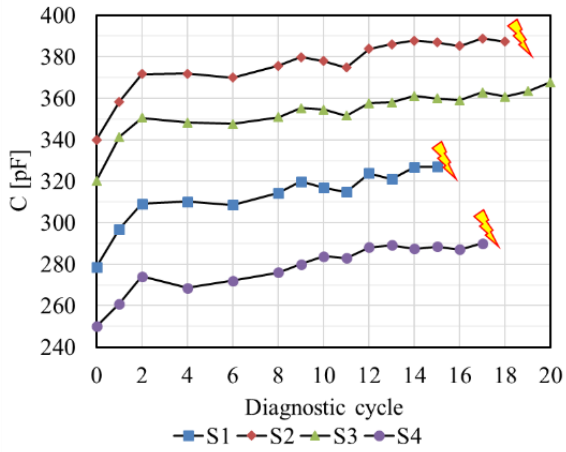

Fig. 10. *Trend of the strand-to-strand IC (at 100 V rms and 50 Hz) over the accelerated aging campaign, for specimens S1÷S4.*

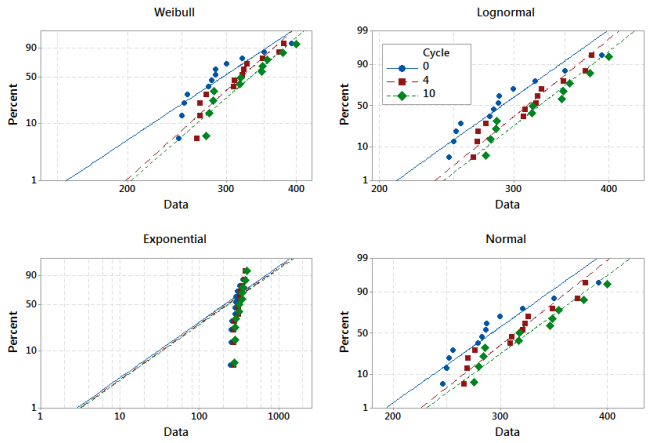

Fig. 11. *Comparison among different probability distribution plots of the strand-to-strand IC measured at 100 V rms and different aging cycles.*

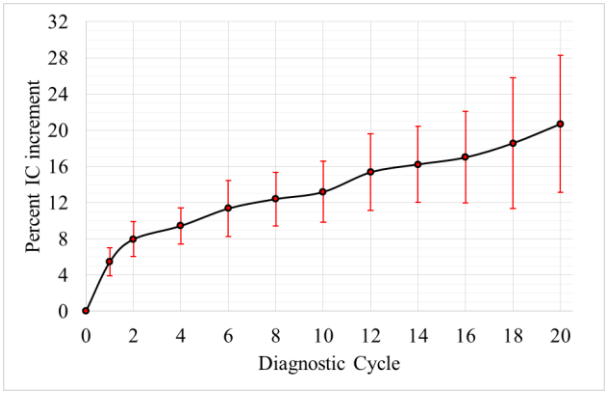

Fig. 12. *Trend of the strand-to-strand IC percent increment (at 100 V rms and 50 Hz) over the accelerated aging campaign, for 12 specimens: a) average value (red dot) and b) standard deviation (red segment).*

Table 2 Specimens Time to Failure

Cycles to failure	Time to failure	Cycles to failure	Time to failure
9	204	18	420
13	300	22	516
15	348	22	516
16	372	23	540
16	372	23	540
17	396	23	540

Over the test campaign, it was observed that the strand-to-strand IC value is independent from the excitation voltage employed during the measurement up to a certain voltage level. As explained in Section 2, the strand-to-strand IC starts to be dependent (i.e. rising) on the applied excitation voltage, when the latter is above the PDIV. Indeed, the PD activity bridges the air-filled voids between the two strands, causing a boost of the detected IC. This behavior is confirmed by the results outlined in Fig. 13, where, for one specimen, the IC values measured at different excitation voltages are plotted over several aging cycles. Only the data regarding one specimen are shown here because a similar trend is identified for all the coils. Analysing the outcomes of Fig. 13, the following considerations can be drawn:

1. for low excitation voltage (<300 V rms), the strand-to-strand IC increases as the specimen becomes more thermally aged, but it is unconstrained by the applied excitation voltage, as previously underlined;
2. the excitation voltage at which the strand-to-strand IC begins to rise, decreases as the thermal aging advances.

The IC increment is indicative of PD activity and the PDIV (i.e. lowest voltage for initiating the PDs) lessens as the aging cycles progress [18]. In particular, the PDIV is above 480 V rms at the end of the first aging session; whilst its value significantly drops below 360 V rms after 20 aging cycles. For both IC magnitude and PDIV value, a significant divergence is appreciable among the different aging cycles, as underlined in Fig. 13. The only anomaly to this general tendency is represented by the cycle '12', which approximately reveals the same trend and absolute IC values as per cycle '16'. This anomaly might have been caused by a non-perfect physical clamping of the coil terminals during the measurements and/or any mishandling of the specimen during the diagnostic cycle.

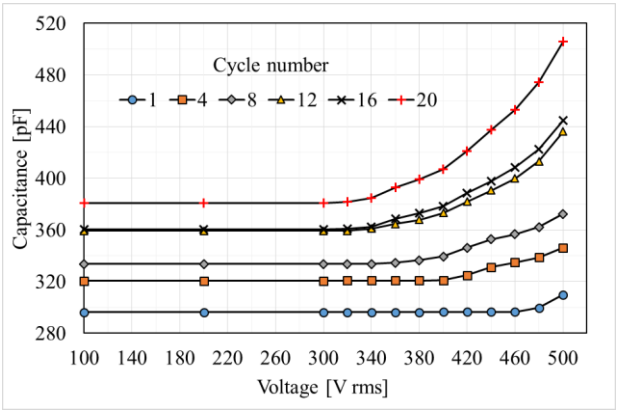

Fig. 13. *Trend of the strand-to-strand IC measured at several excitation voltages, for different aging cycles (the data refer to the same specimen).*

Assuming as reference the IC measured at 100 V rms, the strand-to-strand IC percent increment (i.e. %IC) is determined for a single specimen under several conditions (i.e. excitation voltage and aging cycle). The obtained results are summarized in Fig. 14 and a linear relationship is found between %IC and thermal aging (i.e. the %IC linearly rises with the number of aging cycles).

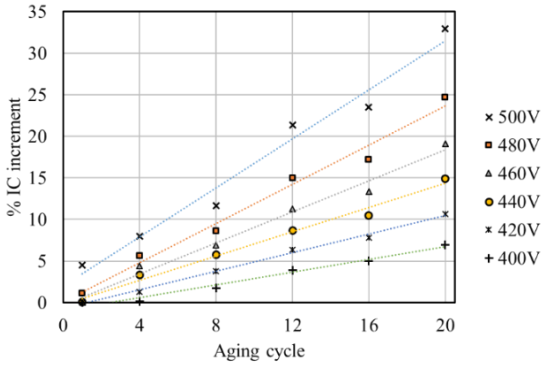

Fig. 14. *Trend of the strand to strand IC percent increment (with respect to IC measured at 100 V rms), for different excitation voltages and aging cycles (the data refer to a single specimen).*

4.2. Dissipation Factor

At excitation voltage lower than the PDIV (e.g. 100 V rms), the strand-to-strand tanδ, measurements are strongly influenced by the ambient RH (see Fig. 9). Therefore, these data cannot be used for establishing a direct relationship between thermal aging and strand-to-strand tanδ absolute value, since the impact of both RH and thermal aging is difficult to be discerned through low excitation voltages. On the other hand, the strand-to-strand tanδ measurements disclose a clear trend with thermal degradation, when excitation voltages above the PDIV are considered. In these conditions (i.e. higher excitation voltage), the variability of the tanδ values, caused by the ambient RH, is 'eclipsed' by the thermal aging effect.

To determine the most appropriate probability distribution that better fits the specimens' strand-to-strand tanδ measurements, a preliminary post-processing analysis has been carried out, as per IC measurements. Its outcomes are recapped in Fig. 15, where four different distributions are compared (i.e. Weibull, exponential, normal and lognormal). Based on Fig. 15's results, the lognormal distribution is selected due to its suitable fitting characteristics. For all specimens, the mean value of %tanδ (measured at 500 V rms) and the standard deviation have been obtained at each diagnostic cycle relying on the lognormal distribution, as shown in Fig. 16. From this figure, the increment of strand-to-strand tanδ with thermal aging is clearly visible.

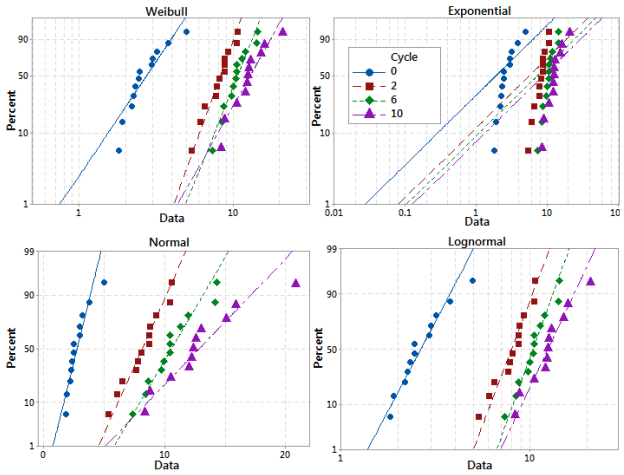

Fig. 15. *Comparison among different probability distribution plots of the strand-to-strand %tanδ measured at 500 V rms and different aging cycles.*

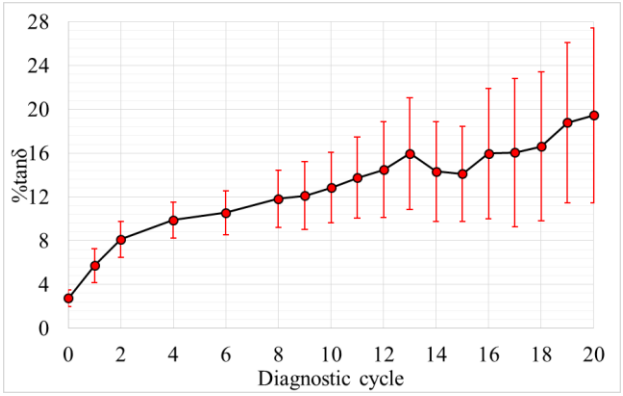

Fig. 16. *Mean value and standard deviation of the strand-to-strand %tanδ measured at 500 V rms for different diagnostic cycles, considering a lognormal distribution.*

The strand-to-strand tanδ depends on the employed excitation voltage and its trend is similar to the one found for the IC measurements. For excitation voltages up to the PDIV, the strand-to-strand tanδ does not significantly vary. On the contrary, considerable variations are observed for excitation voltages above the PDIV, due to the ionization of the air voids. The described trend is illustrated in Fig. 17, where the %tanδ of the same specimen is plotted against the excitation voltage, for different diagnostic cycles. This figure also highlights the twofold effect played by the thermal aging: 1) reduction of the PDIV with the aging progression; and 2) great increment of the tanδ for high excitation voltage (i.e. above the PDIV). Contrarily to the behavior exhibited by the strand-to-strand IC (see Fig. 13), the corresponding tanδ at low voltage (i.e. below the PDIV) is only slightly influenced by the thermal aging. Indeed, the curves of Fig. 17 are almost overlapped for excitation voltages below 320 V rms independently from the aging cycle.

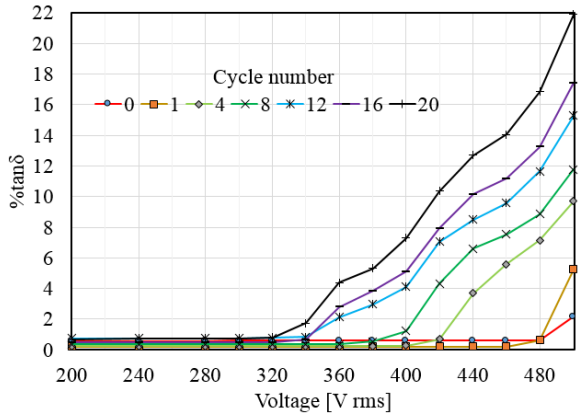

Fig. 17. *Variation of the strand-to-strand %tanδ with the excitation voltage at different aging cycles for the same specimen.*

4.3. Differential Dissipation Factor

For solid insulating materials, it is common practice to evaluate the tanδ increment at two designated voltages (i.e. Δtanδ). As explained in Section 2, this technique is generally used for identifying the level of insulation degradation and it is widely adopted for medium to high voltage insulation systems. However, it is also true that this methodology can also be applied to low voltage insulation systems, as has been shown in this work. Considering the data acquired throughout the test campaign, the strand-to-strand tanδ is measured at different voltage levels (i.e. 0 to 500 V rms with steps of 20 V rms); hence, several Δtanδ can be defined. For convenience, the excitation voltages of 100 V rms and 500 V rms are chosen for determining the $\Delta\tan\delta_{(500\text{-}100)}$ (i.e. tanδ measured at 500 V rms minus the one at 100 V rms). The $\Delta\tan\delta_{(500\text{-}100)}$ values are calculated for several diagnostic cycles and the lognormal probability plot is given in Fig. 18. For sake of completeness, both the mean value and standard deviation of the $\Delta\tan\delta_{(500\text{-}100)}$ lognormal distribution are provided in Fig. 19 and as expected, the $\Delta\tan\delta_{(500\text{-}100)}$ mean value rises with the aging cycles number, because of the progressive insulation degradation.

A sensitivity analysis is also performed on the Δtanδ by changing the considered upper voltage level. In particular, the upper voltage is reduced from 500 to 460 V rms, while keeping the same lower voltage level (i.e. 100 V rms). In Fig. 20, the results corresponding to $\Delta\tan\delta_{(460\text{-}100)}$ are outlined in terms of mean value and standard deviation of the lognormal distribution.

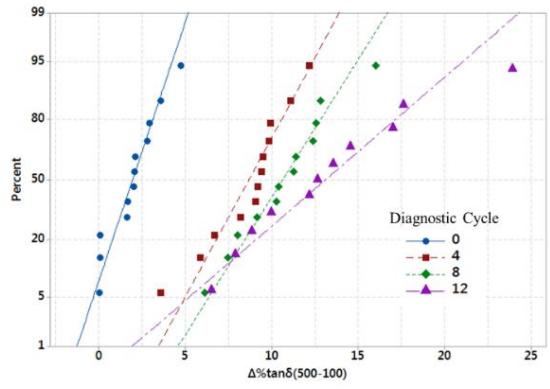

Fig. 18. *Lognormal probability plot of the strand to strand $\Delta\tan\delta_{(500\text{-}100)}$ at several diagnostic cycles.*

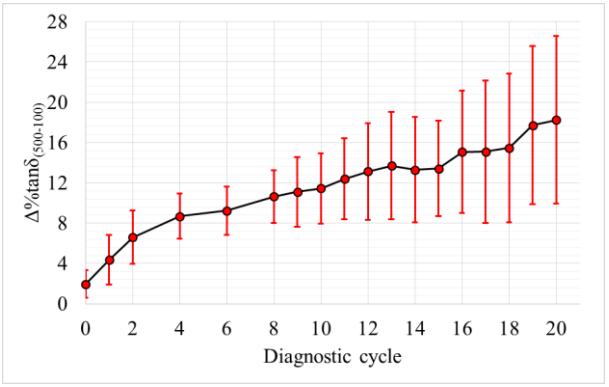

Fig. 19. *Mean value and standard deviation of the $\Delta\tan\delta_{(500\ 100)}$ for different aging cycles.*

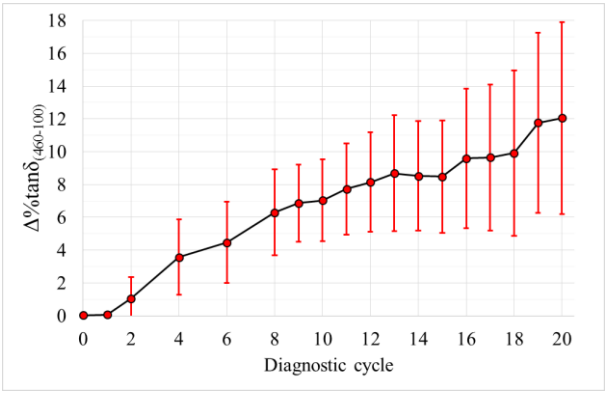

Fig. 20. *Mean value and standard deviation of the $\Delta\tan\delta_{(460\text{-}100)}$ for different aging cycles.*

Likewise the trend obtained using $\Delta\tan\delta_{(500\text{-}100)}$, the $\Delta\tan\delta_{(460\text{-}100)}$ mean value increases at higher aging cycles. However, the $\Delta\tan\delta_{(460\text{-}100)}$ mean values are lower with respect to the $\Delta\tan\delta_{(500\text{-}100)}$ case (see Fig. 19). This mismatch confirms that reducing the excitation voltage amplitude leads to a lower number of ionized voids within the insulation.

4.4. Direct measurement of PDIV

In low voltage EMs, the strand-to-strand IC and tanδ measurements are not generally employed for PDIV assessment, despite their correlation with PD activity. In order to experimentally confirm the link between the obtained results (i.e. IC and tanδ) and the PD inception, a direct measurement of PDIV is carried out. This work is done by using a commercial PD detector (i.e. Techimp® PD-Base II) alongside with a programmable high-voltage power supply (i.e. GW Instek GPT-9000). The test equipment and its setup are shown in Fig. 21, whilst a set of 12 coils, whose arrangement relies on the specifications listed in Table 1, represents the samples' population. Each coil is fed through the programmable power supply and the applied excitation voltage is ramped-up until PDs are incepted. Since PDs emit electromagnetic signals, a high-frequency transverse electromagnetic antenna is used as PD sensor. Once the PDs are detected, the corresponding voltage value (i.e. PDIV) is recorded together with the PD phase resolved pattern generated by a dedicated software. The PDIV values obtained by both PD detector (i.e. direct measure) and dissipation factor tester (i.e. indirect measure based on IC and tanδ) are compared. The results are reported in Fig. 22. The outcome of this analysis reveals that the PDIV values which are directly measured, match the ones estimated through an indirect method (i.e. tanδ and IC). The good agreement

among the PDIV values is also confirmed for different thermal aging levels, which is also illustrated in Fig. 22. Considering these results, it can be safely concluded that the PDIV detection using the dissipation factor tester (i.e. Megger® Delta4000) represents an alternative and more straightforward solution for fast insulation assessment. In fact, the measurements are appropriately accurate, even though an indirect method is used, which traditionally is considered a less accurate methodology. Another perceived advantage of this methodology is the portable nature of the whole setup. The dissipation factor tester physically comprises the required high-voltage power supply as well as the measurement and post-processing tool, thus ensuring equipment portability. Also, it is worth to underline that the data collected with the dissipation factor tester are not affected by ambient noise, which usually plays an important role as source of interference, during measurements performed through a PD detector

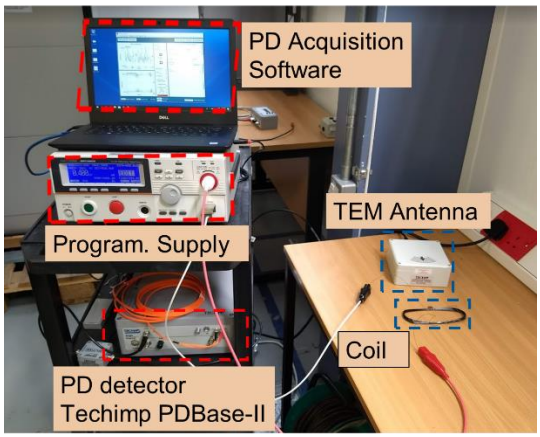

Fig. 21. *Experimental setup for PDIV measurement on random wound coil.*

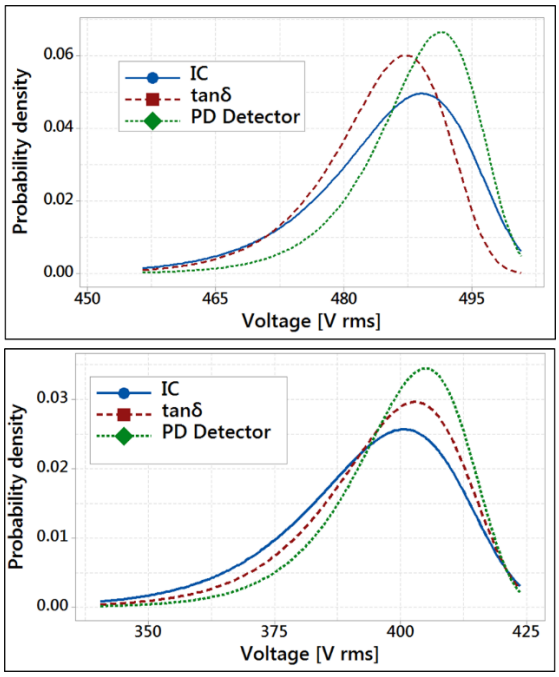

Fig. 22. *Comparison between direct and indirect PDIV measurement (Weibull density) for unaged (top sub-plot) and thermally aged (bottom sub-plot) specimens.*

5. Application of the Study

The change in both IC and Δtanδ indicates the progressive deterioration of the magnet wire dielectric properties. These diagnostic quantities have been investigated and their marked variation depending on the considered diagnostic cycles has been pointed out. The gathered information can then be used to propose an EM design process that includes the insulation lifetime consumption, as a main design objective function. Traditionally, EMs developed for transport applications are designed aiming at two main targets, namely 1) reduced size and 2) excellent reliability. These goals are usually conflicting, since historically reliability is achieved by some measures of over-engineering. The proposed methodology intends to reduce the reliance on the over-engineering approach which will then have a direct benefit also on the EM weight and size.

In this work, the focus has been put on EMs working in short-term overload conditions. This operating mode is ordinary in electromechanical actuator for aerospace applications [35, 36].

Analysing the specimens' time to failure listed in Table 1, the first coil failure is recorded at the 9th diagnostic cycle whereas increments of about 13% and 11% are respectively registered on the %IC and $\Delta\%\tan\delta_{(500\text{-}100)}$, with respect to the diagnostic cycle '0'. The first coil's time to failure corresponds to 204 h of aging above the thermal class, which is equivalent to 9500 applications of the temperature profile shown Fig. 6. This critical information describes the thermal insulation lifetime consumption to a great level of detail. Hence, considering an EM operating according to the Fig. 6 temperature profile, the first winding failure will occur after 9500 thermal overload cycles, in the worst-case scenario. Therefore, combining the thermal aging knowledge associated to a specific mission profile together with the EM thermal model (e.g. lumped parameter thermal network), the EM design process will be significantly enhanced. In fact, by knowing the time to failure and/or level of thermal aging, the EM can be designed and optimized for meeting the predetermined lifetime requirement, while ensuring performance and weight constraints.

For this reason, the presented results along with the mentioned design strategy can support, EM designers in making reliability a design objective function at all stages of the design process. The traditional over-engineering philosophy, usually associated with improving robustness and reliability can thus be reduced or even eliminated completely. Additionally, by including the thermal aging data at the EM design stage, the reliability will no longer be a feature to be evaluated on the final product through statistical methods, but it will truly become a design objective assessed right from the beginning of the project. Finally another perceived advantage of this work is its potential in terms of employing the collected data for EM diagnostic purposes. This can be used to develop improved and better maintenance schedules and thus reduce overall system down-time.

6. Conclusions

This paper examined the effects of thermal ageing on windings and coils used in low voltage EMs, primarily designed for operation with short-term overloaded mission profiles. The impact of thermal aging on both IC and tanδ was experimentally evaluated through a purposely designed

accelerated aging test campaign and a detailed data post-processing.

For excitation voltages lower than the PDIV (<300 V), the following outcomes were found:

1) the IC proportionally rises with the thermal aging level;

2) the tanδ is unaffected by the thermal deterioration of the enamel.

In case of excitation voltage values above the PDIV (300 V<*V*<500 V), it was shown that both IC and tanδ increase with the thermal exposure hours. In particular, the Δtanδ considerably arises with the thermal degradation, indicating a prominent PD activity. It is worth to mention that although high excitation voltages permit to record useful information on the insulation status, they also electrically overstress the enamel layer (i.e. Type I insulation) due to the PD inception. The correlation between diagnostic measurements (i.e. IC and tanδ) and PDIV was proven via a direct detection of PDs and a good agreement among the PDIV values, collected under different methodologies, was revealed.

The influence of ambient RH on the IC and tanδ measurements was also accounted during the test campaign by the adoption of two 'reference specimens'. As outcome of this investigation, it was observed that the strand-to-strand tanδ is very sensitive to the ambient RH. Hence, it is recommended to perform these readings inside a humidity-controlled environment for avoiding misleading results.

Finally, the methodology to integrate the test campaign outcome in the EM design was outlined. The proposed approach enables the trade-off between design for performance and design for reliability, avoiding the insulation over-engineering.

7. Acknowledgments

This work was funded by the INNOVATIVE doctoral programme. The INNOVATIVE programme is partially funded by the Marie Curie Initial Training Networks (ITN) action (project number 665468) and partially by the Institute for Aerospace Technology (IAT) at the University of Nottingham.

This work was also partially funded by the University of Nottingham's Propulsion Futures Beacon through Grant PF42.

This work was also supported by the Ningbo 3315 Innovation Team Scheme under Grant 2018A-08-C .

8. References

[1] G. C. Stone, I. Culbert, E. A. Boulter, and H. Dhirani, *Electrical Insulation for Rotating Machines: Design, Evaluation, Aging, Testing, and Repair*: Wiley, 2014.

[2] A. M. E.-. Refaie, J. P. Alexander, S. Galioto, P. B. Reddy, K. K. Huh, P. d. Bock, *et al.*, "Advanced High-Power-Density Interior Permanent Magnet Motor for Traction Applications," *IEEE Transactions on Industry Applications,* vol. 50, pp. 3235-3248, 2014.

[3] V. Madonna, P. Giangrande, and M. Galea, "Electrical Power Generation in Aircraft: review, challenges and opportunities," *IEEE Transactions on Transportation Electrification,* vol. 4, pp. 646 - 6591, 2018.

[4] V. Madonna, P. Giangrande, A. Walker, and M. Galea, "On the Effects of Advanced End-Winding Cooling on the Design and Performance of Electrical Machines," in *2018 XIII International Conference on Electrical Machines (ICEM)*, 2018, pp. 311-317.

[5] A. Al-Timimy, P. Giangrande, M. Degano, Z. Xu, M. Galea, C. Gerada, *et al.*, "Design and Losses Analysis of a High Power Density Machine for Flooded Pump Applications," *IEEE Transactions on Industry Applications,* pp. 1-1, 2018.

[6] V. Madonna, P. Giangrande, C. Gerada, and M. Galea, "Thermal analysis of fault-tolerant electrical machines for aerospace actuators," *in press on IET Electric Power Applications, DOI: 10.1049/iet-epa.2018.5153,* 2018.

[7] N. Lahoud, J. Faucher, D. Malec, and P. Maussion, "Electrical Aging of the Insulation of Low-Voltage Machines: Model Definition and Test With the Design of Experiments," *IEEE Transactions on Industrial Electronics,* vol. 60, pp. 4147-4155, 2013.

[8] P. Mancinelli, S. Stagnitta, and A. Cavallini, "Qualification of Hairpin Motors Insulation for Automotive Applications," *IEEE Transactions on Industry Applications,* vol. 53, pp. 3110-3118, 2017.

[9] C. Zoeller, M. A. Vogelsberger, R. Fasching, W. Grubelnik, and T. M. Wolbank, "Evaluation and Current-Response-Based Identification of Insulation Degradation for High Utilized Electrical Machines in Railway Application," *IEEE Transactions on Industry Applications,* vol. 53, pp. 2679-2689, 2017.

[10] V. Madonna, A. Walker, P. Giangrande, G. Serra, C. Gerada, and M. Galea, "Improved Thermal Management and Analysis for Stator End-Windings of Electrical Machines," *IEEE Transactions on Industrial Electronics,* vol. 66, pp. 5057-5069, 2019.

[11] S. Grubic, J. M. Aller, B. Lu, and T. G. Habetler, "A Survey on Testing and Monitoring Methods for Stator Insulation Systems of Low-Voltage Induction Machines Focusing on Turn Insulation Problems," *IEEE Transactions on Industrial Electronics,* vol. 55, pp. 4127-4136, 2008.

[12] C. Sciascera, M. Galea, P. Giangrande, and C. Gerada, "Lifetime consumption and degradation analysis of the winding insulation of electrical machines," in *8th IET International Conference on Power Electronics, Machines and Drives (PEMD 2016)*, 2016, pp. 1-5.

[13] P. Giangrande, A. Galassini, S. Papadopoulos, A. Al-Timimy, G. L. Calzo, M. Degano, *et al.*, "Considerations on the Development of an Electric Drive for a Secondary Flight Control Electromechanical Actuator," *in press on IEEE Transactions on Industry Applications,* 2019.

[14] S. A. Bhumiwat, "Depolarization index for dielectric aging indicator of rotating machines," *IEEE Transactions on Dielectrics and Electrical Insulation,* vol. 22, pp. 3126-3132, 2015.

[15] M. Farahani, H. Borsi, and E. Gockenbach, "Study of Capacitance and Dissipation Factor Tip-Up to Evaluate the Condition of Insulating Systems for High Voltage Rotating Machines," *Electrical Engineering,* vol. 89, pp. 263-270, 2007.

[16] F. T. Emery, "Partial discharge, dissipation factor, and corona aspects for high voltage electric generator stator bars and windings," *IEEE Transactions on Dielectrics and Electrical Insulation,* vol. 12, pp. 347-361, 2005.

[17] M. Farahani, H. Borsi, E. Gockenbach, and M. Kaufhold, "Partial discharge and dissipation factor behavior of model insulating systems for high voltage rotating machines under different stresses," *IEEE Electrical Insulation Magazine,* vol. 21, pp. 5-19, 2005.

[18] "IEEE Recommended Practice for Measurement of Power Factor Tip-Up of Electric Machinery Stator Coil Insulation," *IEEE Std 286-2000,* pp. i-29, 2001.

[19] P. Werynski, D. Roger, R. Corton, and J. F. Brudny, "Proposition of a new method for in-service monitoring of the aging

of stator winding insulation in AC motors," *IEEE Transactions on Energy Conversion,* vol. 21, pp. 673-681, 2006.

[20] J. Yang, J. Cho, S. B. Lee, J. Y. Yoo, and H. D. Kim, "An Advanced Stator Winding Insulation Quality Assessment Technique for Inverter-Fed Machines," *IEEE Transactions on Industry Applications,* vol. 44, pp. 555-564, 2008.

[21] D. Bogh, J. Coffee, G. Stone, and J. Custodio, "Partial-discharge-inception testing on low-voltage motors," *IEEE Transactions on Industry Applications,* vol. 42, pp. 148-154, 2006.

[22] M. Tozzi, A. Cavallini, and G. C. Montanari, "Monitoring off-line and on-line PD under impulsive voltage on induction motors - Part 2: testing*," *IEEE Electrical Insulation Magazine,* vol. 27, pp. 14-21, 2011.

[23] A. Cavallini, D. Fabiani, and G. C. Montanari, "A novel method to diagnose PWM-fed induction motors," *IEEE Transactions on Dielectrics and Electrical Insulation,* vol. 15, pp. 1313-1321, 2008.

[24] P. Wang, H. Xu, J. Wang, W. Wang, and A. Cavallini, "Effect of repetitive impulsive voltage duty cycle on partial discharge features and insulation endurance of enameled wires for inverter-fed low voltage machines," *IEEE Transactions on Dielectrics and Electrical Insulation,* vol. 24, pp. 2123-2131, 2017.

[25] V. Madonna, P. Giangrande, W. Zhao, G. Buticchi, H. Zhang, C. Gerada, *et al.*, "Reliability vs. Performances of Electrical Machines: Partial Discharges Issue," presented at the IEEE WEMDCD'19 - Workshop on Electrical Machines Design, Control and Diagnosis, Athens, Greece, 2019.

[26] M. Farahani, E. Gockenbach, H. Borsi, K. Schafer, and M. Kaufhold, "Behavior of machine insulation systems subjected to accelerated thermal aging test," *IEEE Transactions on Dielectrics and Electrical Insulation,* vol. 17, pp. 1364-1372, 2010.

[27] S. Savin, S. Ait-Amar, and D. Roger, "Turn-to-turn capacitance variations correlated to PDIV for AC motors monitoring," *IEEE Transactions on Dielectrics and Electrical Insulation,* vol. 20, pp. 34-41, 2013.

[28] V. Madonna, P. Giangrande, L. Lusuardi, A. Cavallini, and M. Galea, "Impact of thermal overload on the insulation aging in short duty cycle motors for aerospace," in *2018 IEEE ESARS-ITEC*, 2018, pp. 1-6.

[29] Z. Huang, T. Yang, P. Giangrande, S. Chowdhury, M. Galea, and P. Wheeler, "An Active Modulation Scheme to Boost Voltage Utilization of the Dual Converter With a Floating Bridge," *IEEE Transactions on Industrial Electronics,* vol. 66, pp. 5623-5633, 2019.

[30] ASTM, "D150-18, Standard Test Methods for AC Loss Characteristics and Permittivity (Dielectric Constant) of Solid Electrical Insulation," ed. West Conshohocken, PA: ASTM International, 2018.

[31] A. K. Jonscher, "Dielectric relaxation in solids," *Journal of Physics D: Applied Physics,* vol. 32, p. R57, 1999.

[32] M. Lukic, A. Hebala, P. Giangrande, C. Klumpner, S. Nuzzo, G. Chen, *et al.*, "State of the Art of Electric Taxiing Systems," in *2018 IEEE ESARS-ITEC*, 2018, pp. 1-6.

[33] "IEC 60172:2015 Test procedure for the determination of the temperature index of enamelled and tape wrapped winding wires," ed: IEC, 2015.

[34] "IEC 60505:2011 Evaluation and qualification of electrical insulation systems," ed: IEC, 2011.

[35] G. Qiao, G. Liu, Z. Shi, Y. Wang, S. Ma, and T. C. Lim, "A review of electromechanical actuators for More/All Electric aircraft systems," *Proceedings of the Institution of Mechanical Engineers, Part C: Journal of Mechanical Engineering Science,* vol. 232, pp. 4128-4151, 2018.

[36] P. Giangrande, V. Madonna, S. Nuzzo, and M. Galea, "Design of Fault-Tolerant Dual Three-Phase Winding PMSM for Helicopter Landing Gear EMA," in *2018 IEEE ESARS-ITEC*, 2018, pp. 1-6.